Dissociation of State-Selected NO_2^+ Ions Studied by Threshold Photoelectron−Photoion Coincidence Techniques†

Kazuhiko Shibuya*

Department of Chemistry, Tokyo Institute of Technology, Ohokayama, Meguro, Tokyo 152, Japan

Shinzo Suzuki

Department of Chemistry, Tokyo Metropolitan University, Minami-Ohsawa, Hachioji, Tokyo 159-03, Japan

Takashi Imamura

The National Institute for Environmental Studies, Tsukuba, Ibaraki 305, Japan

Inosuke Koyano

Department of Material Science, Himeji Institute of Technology, Kamigori, Hyogo 678-12, Japan

Received: July 9, 1996; In Final Form: September 30, 1996⊗

Fragmentation patterns and dissociation rates of state-selected NO_2^+ ions were measured by the threshold photoelectron−photoion coincidence (TPEPICO) method in the region of 40−100 nm. Parent NO_2^+ ions were detected when they were prepared in the excited states located above the first dissociation limit (D_0^0 = 2.79 eV), correlating to $NO^+(X^1\Sigma^+) + O(^3P)$. Specially, the dissociation rate (k_{dis}) of NO_2^+ ions in the lowest excited $\tilde{a}^3B_2$ state increases with increasing the quantum number of the bending vibration (n_2): $(7.4 \pm 4.9) \times 10^2$, $(1.32 \pm 0.56) \times 10^3$, $(1.51 \pm 0.40) \times 10^4$, and $(2.38 \pm 0.51) \times 10^4$ s^{-1} for n_2 = 0, 1, 2, and 3, respectively. The branching ratios of two dissociation pathways, $NO^+ + O$ and $O^+ + NO$, were found to depend on the electronic state of the parent ion. The unimolecular dissociation channels are discussed in terms of dissociation potential surfaces open for individual electronic states and radiative relaxation to lower electronic states.

I. Introduction

The photochemistry[1−3] and spectroscopy[4,5] of NO_2 have been well studied. The excited states of NO_2 couple with each other strongly through vibronic and spin−orbit interactions. As a consequence of the strong coupling network, the photoexcited NO_2 lying above the first dissociation limit (25 129 cm^{-1}, 397.9 nm) predissociates very rapidly. The longest dissociative lifetime is 42 ps, which was measured for $\tilde{D}^2B_2$ (0,0,0). The excited state lying 10 cm^{-1} above the first dissociation limit has a short lifetime of 6 ps. The lifetimes become shorter as the excitation energies increase. On the other hand, the photochemistry and spectroscopy of NO_2^+ have not been studied yet.

The equilibrium bond angles of NO_2 and NO_2^+ in their ground electronic states are quite different: 134° for NO_2 and 180° for NO_2^+. This has long been a baffle for the accurate determination of the adiabatic ionization potential (IP) of NO_2 and the experimental investigation on the chemistry and spectroscopy of NO_2^+. Grant and his co-workers have determined the adiabatic IP (77 316 cm^{-1}, 129.340 nm) with the multiphoton ionization method of NO_2 via linear Rydberg states.[6] In single-photon-ionization spectroscopy, the Franck−Condon principle leads to the generation of vibrationally excited NO_2^+ ions alone in the ground state. On the other hand, the ejection of an inner valence electron from NO_2 is Franck−Condon favored due to the geometrical similarity between the ground-state NO_2 and the inner valence hole NO_2^+. Therefore, one can prepare electronically-excited and state-selected NO_2^+ ions by photoionization in the spectral region shorter than 100 nm.

In the present study, this technique has been used to investigate the dissociation mechanisms of the state-selected NO_2^+ ions. We have measured the threshold electron spectrum (TES) of NO_2, the photoionization efficiency (PIE) curves of its parent and fragment ions, and the threshold photoelectron−ion coincidence spectra in the 50−100-nm range using the TEPSICO[7] and TEPSICO-II[8] apparatus.

II. Experimental Section

The apparatus used were TEPSICO and TEPSICO-II, which have been described in detail elsewhere.[7,8] The procedures were the same as those employed in the previous studies of state-selected ion/molecule reactions[7] except that the reactant gas was not introduced into the reaction chamber. The NO_2 molecules were ionized in the ionization chamber by monochromatic vacuum UV radiation from the He Hopfield continuum dispersed by a 1-m Seya−Namioka monochromator (0.05-nm FWHM in the case of TEPSICO) or from synchrotron radiation at the UVSOR facility dispersed by a 3-m normal incidence monochromator (0.02-nm FWHM in the case of TEPSICO-II). The photoelectrons and ions were extracted from the ionization chamber/region by a weak electric field in the direction perpendicular to the photon beam and opposite to each other. The threshold photoelectrons were selected by a non-line-of-sight steradiancy analyzer[9] and allowed to pass to a channel multiplier. The ions were mass analyzed by a quadrupole mass spectrometer and detected by another channel multiplier. These ion signals were then counted in coincidence with the threshold electron signals, thus yielding direct information on the relative abundance of the parent and all fragment ions for various specified internal energies of the parent ions.

† The experimental work was performed at Institute for Molecular Science, Okazaki, Japan.

⊗ Abstract published in *Advance ACS Abstracts,* December 15, 1996.

S1089-5639(96)02031-2 CCC: $14.00

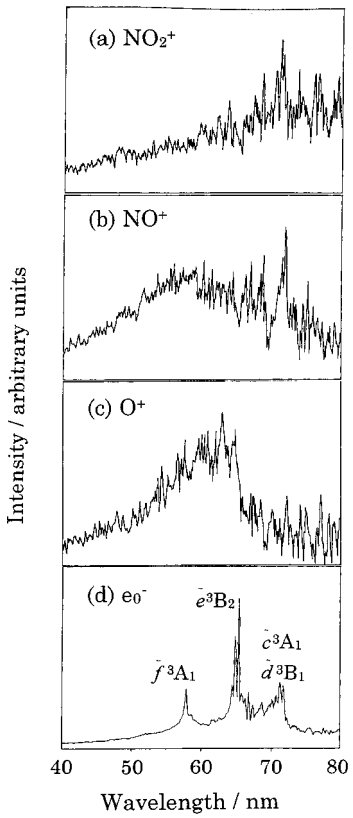

Figure 1. Photoionization efficiency curves and threshold photoelectron spectrum of NO_2 in the range of 40−80 nm. Photoinoization efficiency curves are for (a) NO_2^+, (b) NO^+, and (c) O^+. The assignments of threshold photoelectron spectrum d are taken from ref 10.

III. Results

A. Photoionization Efficiency Curves and Threshold Electron Spectrum. Figure 1 presents three photoionization efficiency curves (a−c) and a threshold photoelectron spectrum (d) of NO_2 in the region of 40−80 nm, which were measured using the TEPSICO-II. The threshold electron spectrum is in accordance with the He I (21.21-eV) and He II (40.82-eV) photoelectron spectra reported by Brundle et al.[10] They assigned the photoelectron spectra based on the SCF calculation of NO_2 and NO_2^+, as well as on the comparison with the ionization potentials of CO_2, which is isoelectronic with NO_2^+. The ground electronic configurations of linear CO_2 and bent NO_2 are presented below:

$$CO_2\tilde{X}^1\Sigma_g^+: \quad \cdots(\sigma_g)^2(\sigma_u)^2 \quad (\pi_u)^4 \quad (\pi_g)^4$$

$$NO_2\tilde{X}^2A_1: \quad \cdots(4a_1)^2(3b_2)^2 \quad (1b_1)^2(5a_1)^2 \quad (1a_2)^2(4b_2)^2 \quad (6a_1)$$

Statistically, ionizations of NO_2 $\tilde{X}^2A_1$ to the triplet states of NO_2^+ should be 3 times as intense as those to the corresponding singlet ionic states.[11] The triplet states of NO_2^+ are mainly recognized in Figure 1d. According to the assignments by Brundle et al.,[10] the triplet states of NO_2^+ prepared by photoionization in the spectral region of 50−100 nm are listed in Table 1. More accurate energy calculation of NO_2 at the equilibrium geometry of the ground state has been carried out by Handy et al.,[12] but they did not report on NO_2^+. We, therefore, accept the assignments by Brundle et al.,[10] which have since been confirmed to be correct by Kimura et al.[13]

In spectrum d, one can recognize three strong bands corresponding to the generation of NO_2^+: c^3A_1, $\tilde{e}^3B_2$, and $\tilde{f}^3A_1$. The 1100-cm^{-1} progression due to the N−O stretch in $\tilde{e}^3B_2$ is seen around 65 nm: The 0−0 band of NO_2^+ $\tilde{e}^3B_2$−NO_2 $\tilde{X}^2A_1$ corresponds to a band at 65.7 nm. The bond angle of NO_2^+ $\tilde{e}^3B_2$ is close to that of NO_2 $\tilde{X}^2A_1$ (134°), and the spectrum does not show the vibrational structure. A similar 1100-cm^{-1} progression of NO_2^+ $\tilde{c}^3A_1$, which is accompanied by a weak progression of $\tilde{d}^3B_1$, is seen around 70 nm: The 0−0 band of NO_2^+ $\tilde{c}^3A_1$−NO_2 $\tilde{X}^2A_1$ is located at 73.0 nm. The NO_2^+ $\tilde{f}^3A_1$−NO_2 $\tilde{X}^2A_1$ transition seen at 58 nm does not have any obvious vibrational structure.

TABLE 1: Summary of the Triplet States of NO_2^+ and Their Adiabatic Ionization Potentials

elec state	adiabatic IP, eV	wavelength, nm
$\tilde{a}^3B_2\ (4b_2)^{-1}$	12.85	96.5
$\tilde{b}^3A_2\ (1a_2)^{-1}$	13.60	91.2
$\tilde{c}^3A_1\ (5a_1)^{-1}$	16.99	73.0
$\tilde{d}^3B_1\ (1b_1)^{-1}$	17.06	72.7
$\tilde{e}^3B_2\ (3b_2)^{-1}$	18.86	65.7
$\tilde{f}^3A_1\ (4a_1)^{-1}$	21.26	58.3

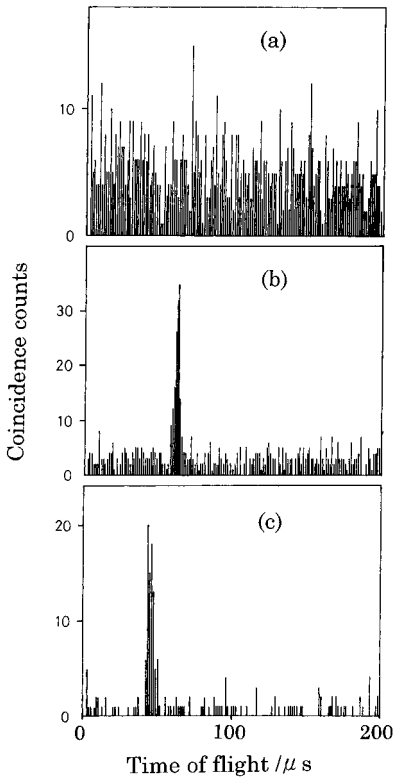

Figure 2. Time-of-flight TEPICO spectra of (a) NO_2^+, (b) NO^+, and (c) O^+ ions generated through the $\tilde{e}^3B_2(0,0,0)$ state of NO_2^+, where NO_2 was photoionized at 65.7 nm.

The photoionization efficiency curves for the parent NO_2^+ and fragment NO^+ and O^+ ions are displayed as spectra a, b, and c, respectively, in Figure 1. Similar photoionization efficiency curves of NO_2^+ have been obtained by Weissler et al.[14] and Dibeler et al.[15] The O^+ production (threshold wavelength = 70.1 nm) was observed in the region shorter than 65 nm, which is in accord with the location of NO_2^+ $\tilde{e}^3B_2$. The NO^+ and NO_2^+ productions (threshold wavelengths = 100.2 and 129.3 nm, respectively) are recognized over the whole spectral region of Figure 1. The distinct NO^+ and NO_2^+ productions via the $\tilde{c}^3A_1$ state are evident.

B. Threshold Electron−Photoion Coincidence. Figure 2 shows the TOF coincidence spectra obtained with excitation at 65.7 nm, corresponding to the preparation of NO_2^+ $\tilde{e}^3B_2$-(n_1,n_2,n_3) = (0,0,0), where n_1, n_2, and n_3 are the vibrational quantum numbers of symmetric stretch, bend, and asymmetric stretch of NO_2^+, respectively. The NO^+ and O^+ ions are

TABLE 2: Branching Ratios of Ionic Products Generated from State-Selected NO_2^+

ionization wavelength, nm	ionic state	ionic products[a] (1) NO_2^+	(2) NO^+	(3) O^+
96.5	$\tilde{a}^3B_2(000)$	0.96 ± 0.43^b	0.04 ± 0.02^b	n.d.[c]
95.9	$\tilde{a}^3B_2(010)$	0.93 ± 0.31^b	0.07 ± 0.02^b	n.d.[c]
95.3	$\tilde{a}^3B_2(020)$	0.44 ± 0.15^b	0.57 ± 0.10^b	n.d.[c]
94.7	$\tilde{a}^3B_2(030)$	0.27 ± 0.08^b	0.73 ± 0.18^b	n.d.[c]
71.5	$\tilde{c}^3A_1(200)$	0.38 ± 0.07^d	0.62 ± 0.06^d	n.d.[c]
65.7	$\tilde{e}^3B_2(000)$	n.d.[c]	0.60 ± 0.07	0.40 ± 0.05
65.3	$\tilde{e}^3B_2(100)$	n.d.[c]	0.65 ± 0.06	0.35 ± 0.04
58.3	$\tilde{f}^3A_1$	n.d.[c]	0.86 ± 0.10	0.14 ± 0.03

[a] The energetical threshold wavelengths are (1) 129 nm for NO_2^+, (2) 100 nm for NO^+, and (3) 70 nm for O^+. [b] Time-of-flight of NO_2^+ was 55 μs. [c] Not detected. [d] Time-of-flight of NO_2^+ was 65 μs.

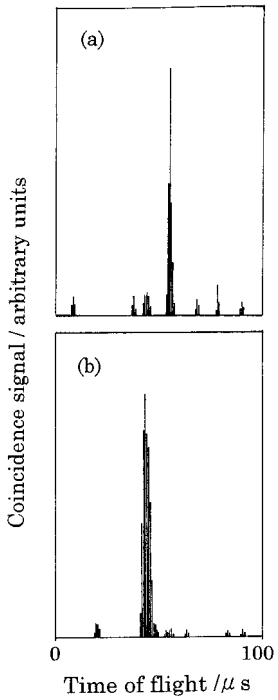

Figure 3. Time-of-flight TEPICO spectra of (a) NO_2^+ and (b) NO^+ ions generated through the $\tilde{a}^3B_2(0,2,0)$ state of NO_2^+, where NO_2 was photoionized at 95.3 nm.

definitely generated via NO_2^+ $\tilde{e}^3B_2(0,0,0)$ as recognized in the coincidence spectra b and c, while the NO_2^+ ion was not detected in spectrum a. The branching ratio of NO^+, $[NO^+]/([NO^+] + [O^+])$, was obtained to be 0.60. Table 2 lists the branching ratios of three product ions, which are normalized to unity of the total ion yield ($[NO_2^+] + [NO^+] + [O^+] = 1$).

From the measurements at 58.3 nm, corresponding to the preparation of NO_2^+ $\tilde{f}^3A_1$, the branching ratio of NO^+ was obtained to be 0.86, which is 43% larger than the ratio derived for NO_2^+ $\tilde{e}^3B_2(0,0,0)$.

In the spectral region longer than 70 nm, the O^+ ions are not generated for energetical reasons. In the measurements at 71.5 nm, corresponding to the preparation of NO_2^+ $\tilde{c}^3A_1(2,0,0)$, only NO_2^+ and NO^+ ions are generated: The branching ratio of NO^+, $[NO^+]/([NO^+] + [NO_2^+])$, was 0.62 under the flight time of $NO_2^+ = 65$ μs.

Figure 3 shows the TOF coincidence spectra obtained with the excitation at 95.3 nm, corresponding to the preparation of NO_2^+ $\tilde{a}^3B_2(0,2,0)$. The branching ratio of NO^+ was 0.57 under the flight time of $NO_2^+ = 55$ μs. The ratio varies monotonously from 0.04 at (0,0,0) to 0.73 at (0,3,0) as listed in Table 2 which implies the apparent dependence of the ratio on the vibrational quantum number, n_2.

IV. Discussion

The NO_2^+ $\tilde{X}^1\Sigma_g^+ - NO_2$ $\tilde{X}^2A_1$ transition band has a Franck−Condon maximum at 110 nm, and the photoionization of NO_2, process 1, occurs mainly by a light of $\lambda = 100-120$ nm.[6] The

$$NO_2 + h\nu \rightarrow NO_2^+ \tilde{X}^1\Sigma_g^+ + e^- \quad \lambda \leq 129.3 \text{ nm} \quad (1)$$

NO_2^+ ions prepared in this way are vibrationally hot, especially in the bending mode. The possible processes of the dissociative photoionization are summarized as processes 2−5. We detected

$$NO_2 + h\nu \rightarrow NO^+(X^1\Sigma^+) + O(^3P) + e^- \quad \lambda \leq 100.2 \text{ nm} \quad (2)$$

$$NO_2 + h\nu \rightarrow O_2^+(X^2\Pi_g) + N(^4S) + e^- \quad \lambda \leq 74.8 \text{ nm} \quad (3)$$

$$NO_2 + h\nu \rightarrow O^+(^4S) + NO(X^2\Pi) + e^- \quad \lambda \leq 70.1 \text{ nm} \quad (4)$$

$$NO_2 + h\nu \rightarrow N^+(^3P) + O_2(X^3\Sigma_g^-) + e^- \quad \lambda \leq 65.2 \text{ nm} \quad (5)$$

ion signals of NO_2^+, NO^+, and O^+ but could not measure those of O_2^+ and N^+ in the present experiment by the photoionization of NO_2 in the range of 50−100 nm. Processes 3 and 5 are not important. Dibeler et al. measured the relative intensities of NO_2^+, NO^+, O^+, and N^+ ions with photoionization at 58.4 nm to be 0.49, 1.0, 0.18, and 0.003, respectively.[14] In fact, the N^+ signal is 2 orders of magnitude weaker than the other ion signals. Process 3 has not yet been measured experimentally. In the following sections, we discuss processes 2 and 4.

The ground state of NO_2^+ is $\tilde{X}^1\Sigma_g^+$ (or $^1A_1$), having a linear geometry and an electron configuration of $\cdots 4(\sigma_g)^2(3\sigma_u)^2(1\pi_u)^4(1\pi_g)^4$, which is the same configuration as that of CO_2 $\tilde{X}^1\Sigma_g^+$. The dissociation energy (D_0^0) of $O-NO^+$ is 2.79 eV. The first excited triplet state of NO_2^+ is $\tilde{a}^3B_2$, which is bent ($\theta = 120°$)[10] and lies 3.21 eV above $\tilde{X}^1\Sigma_g^+$. Therefore, NO_2^+ $\tilde{a}^3B_2$ is energetically possible to decompose into $NO^+(X^1\Sigma^+)$ and $O(^3P)$. Actually, we observed the dissociation product NO^+ as can be recognized in Figure 3, where the coincidence signals of NO_2^+ and NO^+ were generated through NO_2^+ $\tilde{a}^3B_2(0,2,0)$ prepared with the photoionization of NO_2 at 95.3 nm. In this spectral region, the formation of NO_2^+ in the vibrationally-excited $\tilde{X}^1\Sigma_g^+$ through process 1 is negligible due to the Franck−Condon principle.[6] One can recognize that the NO^+ signal peaking at 44 μs is broader than the NO_2^+ signal. This observation originates from the fact that NO_2^+ $\tilde{a}^3B_2(0,2,0)$ decomposes through process 2 during the flight time of 55 μs. Assuming single-exponential decay and neglecting the phosphorescing decay NO_2^+ $\tilde{a}^3B_2 \rightarrow \tilde{X}^1\Sigma_g^+$, the unimolecular dissociation rate (k_{dis}) is estimated by

$$k_{dis} = \frac{1}{TOF} \ln\left(1 + \frac{NO^+ \text{ signal}}{NO_2^+ \text{ signal}}\right) \quad (6)$$

where TOF is 55 μs. For example, the k_{dis} value of NO_2^+ $\tilde{a}^3B_2(0,2,0)$ is calculated to be $(1.51 \pm 0.40) \times 10^4$ s^{-1}, corresponding to a lifetime (τ) of 66 μs. In the same way, the dissociation rates and lifetimes of NO_2^+ $\tilde{a}^3B_2(0,n_2,0)$ are obtained as summarized in Table 3. The dissociation rates are also plotted as a function of the n_2 quantum number in Figure 4. We have no available data on the phosphorescence decay of NO_2^+ $\tilde{a}^3B_2 \rightarrow \tilde{X}^1\Sigma_g^+$, but the $\tilde{a}^3B_2 \rightarrow \tilde{X}^1\Sigma_g^+$ phosphorescence lifetime of isoelectronic CO_2 is reported as 570 ms,[16] which is 500 times longer than the longest dissociation lifetime (1.35 ms). Thus,

TABLE 3: Coincidence Signals, Dissociation Rates, and Lifetimes of NO_2^+ $\tilde{a}^3B_2(0,n_2,0)$

	n_2			
	0	1	2	3
NO_2^+ signal/counts	100 ± 32	170 ± 41	100 ± 32	21 ± 5
NO^+ signal/counts	4 ± 2	12 ± 3	130 ± 11	58 ± 11
$k_{dis}/10^3$ s^{-1}	0.74 ± 0.49	1.32 ± 0.56	15.1 ± 4.0	23.8 ± 5.1
τ/ms	$1.35 \pm 2.7/1.3$	$0.76 \pm 0.56/0.23$	$0.066 \pm 0.024/0.014$	$0.042 \pm 0.009/0.007$

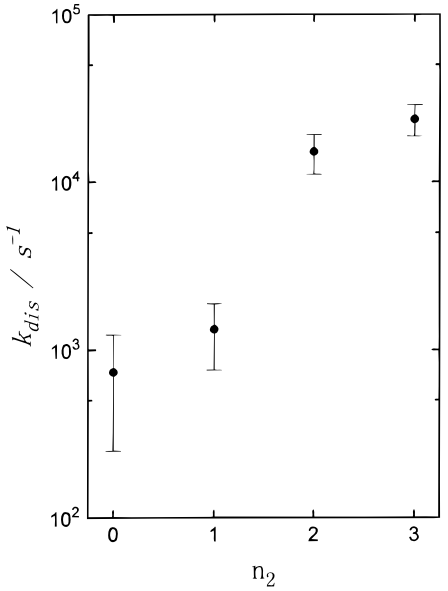

Figure 4. Dissociative decay rate (k_{dis}) of NO_2^+ in the $\tilde{a}^3B_2$ state as a function of quantum numbers of the bending vibration.

one can safely neglect the radiative decay of NO_2^+ $\tilde{a}^3B_2$. By measuring the relative intensities of metastable NO_2^+ signals in the photoionization efficiency curves of NO_2, Chupka estimated the dissociation lifetimes of NO_2^+ $\tilde{a}^3B_2(0,n_2,0)$ as follows:[17] $\tau \geq 150$ μs for $n_2 = 0$, $\tau = 55$ μs for $n_2 = 1$, $\tau = 15$ μs for $n_2 = 2$, $\tau \leq 5$ μs for $n_2 = 3$. Chupka's lifetime values are 1 order of magnitude shorter than ours but almost parallel ours. We believe that the coincidence experiment gives more accurate lifetime values, because the photoelectron−photoion coincidence techniques are assured to detect the fragment ion signals originating with NO_2^+ $\tilde{a}^3B_2(0,n_2,0)$.

An important question to be addressed, then, is why NO_2^+ $\tilde{a}^3B_2$ dissociates into NO^+ and $O(^3P)$ so slowly (at rates of 7×10^2−2×10^4 s^{-1}). The $\tilde{a}^3B_2(0,0,0)$ state lies 0.47 eV above the dissociation limit of $NO^+(X^1\Sigma^+) + O(^3P)$, which correlates with three triplet states of NO_2^+, including $^3B_2$. Eland proposed a tunneling mechanism in which NO_2^+ $\tilde{a}^3B_2$ predissociates through a barrier formed by an avoided crossing of the NO_2^+ $\tilde{a}^3B_2$ potential and a repulsive $^3B_2$ surface correlating with $NO^+(X^1\Sigma^+) + O(^3P)$.[18] This mechanism deserves attention, because the tunneling of the oxygen atom, an atom heavier than hydrogen, is not well-known. The slow dissociation processes of the state-selected excited molecule proceeding at rates of 10^3 s^{-1} have seldom been reported and may be interpreted in terms of classical tunneling. Therefore, we tried to analyze the dissociation rate by fitting the classical tunneling formula of a parabolic barrier[12]

$$k_{\mathrm{dis}} = \nu \exp\left\{-\beta\left(1 - \frac{W}{E}\right)\right\} \tag{7}$$

$$\beta = \frac{\pi\alpha}{\hbar}\sqrt{2\mu E} \tag{8}$$

where ν is the vibrational frequency, α thickness of the barrier (HWHM), μ reduced mass, E barrier height, and W vibrational energy. As recognized in Figure 4, the dissociation rate might depend exponentially on the vibrational energy. From eq 7,

$$\ln k_{\mathrm{dis}} = \ln \nu - \beta + \left(\frac{\beta}{E}\right)W \quad \text{for } W < E \tag{9}$$

is derived and $k_{\mathrm{dis}} = \nu$ for $W > E$. Assuming a tunneling model, the slope of the data plotted in Figure 4 gives the β/E value of 1.78×10^{-3} cm. On the other hand,

$$\frac{\beta}{E} = \frac{\pi\alpha}{\hbar}\sqrt{\frac{2\mu}{E}} = 0.025\,\frac{\alpha/\mathrm{pm}}{\sqrt{E/\mathrm{cm}^{-1}}}\,\mathrm{cm} \tag{10}$$

is calculated by simply introducing the necessary constants. By combining the experimentally obtained ratio of $\beta/E = 1.78 \times 10^{-3}$ cm and eq 10,

$$\sqrt{E/\mathrm{cm}^{-1}} = 13.8(\alpha/\mathrm{pm}) \tag{11}$$

is obtained as a relation between barrier height and thickness. If the top of the barrier is assumed to be at the $\tilde{a}^3B_2(0,4,0)$ level, or $E = 2925$ cm^{-1}, the thickness of the barrier (α) and vibrational frequency (ν) are calculated to be 4 pm and 10^5 s^{-1}, respectively. These values are abnormally small and not reasonable. Even if one adjusts the vibrational frequency to be 10^{13} s^{-1}, the other parameters become $E = 7300$ cm^{-1} and $\alpha = 6$ pm, which are again not reasonable as a tunneling barrier. Thus, we conclude that the simple classical tunneling mechanism cannot explain a variation in the slow dissociation rate of NO_2^+ $\tilde{a}^3B_2(0,n_2,0)$.

There are no available data to be compared with our present results on the dissociation of state-selected NO_2^+ $\tilde{a}^3B_2(0,n_2,0)$. A more accurate theoretical analysis will be required to understand the slow and n_2-dependent dissociation rate. An alternative dissociation route might be expressed as NO_2^+ $\tilde{a}^3B_2$ → NO_2^+ $\tilde{X}^1\Sigma_g^+$ → $NO^+(X^1\Sigma^+) + O(^3P)$, which assumes intermediacy of vibrationally-excited NO_2^+ $\tilde{X}^1\Sigma_g^+$ and may explain the slow dissociation rates. This intersystem crossing mechanism is, however, not likely judging from the fact that the phosphorescence lifetime of isoelectronic CO_2 $\tilde{a}^3B_2$ (570 ms)[16] is 500 times longer than the longest dissociation lifetime of NO_2^+ $\tilde{a}^3B_2$ (1.35 ms). The photodissociation of isoelectronic CO_2 has been reported by a few research groups. Slanger and Black determined the quantum yield of oxygen atom to be unity in the photolysis of CO_2 at 147.0 and 130.2−130.6 nm.[19] The yields of $O(^1D)$ and $O(^3P)$ are 0.94 and 0.06, respectively, with the irradiation at 157 nm.[20] The dissociation dynamics on the $^1B_2$ surface are discussed by Miller et al. from their experiment on the product-state distribution of CO_2.[21] However, the photodissociation of triplet CO_2 has not been studied so for due to the extremely weak absorption of the singlet−triplet transition.

The third excited triplet state of NO_2^+, $\tilde{c}^3A_1$, lies 0.26 eV above the dissociation limit of $O^+(^4S) + NO(X^2\Pi)$. However, we could not detect coincidence signals of O^+ with the photoionization of NO_2 to NO_2^+ $\tilde{c}^3A_1$. This is reasonable considering the fact that a $^3A_1$ surface does not arise from O^+-

(^4S) + NO($X^2\Pi$). On the other hand, we detected the coincidence ion signals of parent NO_2^+ ions in addition to those of the fragment NO^+. It is surprising to detect the parent ions of NO_2^+ after such a long flight time as 65 μs, because the $\tilde{c}^3A_1$ state lies 4.61 eV above the first dissociation limit of NO^+-($X^1\Sigma^+$) + O(^3P). Taking an example of neutral NO_2, the longest-lived excited state among those existing above the first dissociation limit is $\tilde{D}^2B_2$ with a lifetime of 42 ps. How can NO_2^+ $\tilde{c}^3A_1$ be alive as long as 65 μs? A clue to answer this question seems to exist in the magnitude of the dissociation lifetime of 67 μs, which is calculated by applying eq 6 to the data obtained for NO_2^+ $\tilde{c}^3A_1(0,2,0)$. In the coincidence TOF spectrum, the width of the fragment NO^+ peak is broader than that of the parent NO_2^+ peak. This is essentially the same observation as in the TOF spectrum at 95.3 nm, shown in Figure 3. More surprisingly, the dissociation lifetime of $\tilde{c}^3A_1(0,2,0)$ agrees well with that of $\tilde{a}^3B_2(0,2,0)$, 66 μs. On the basis of these observations, we propose a radiative relaxation mechanism to explain the long lifetime of NO_2^+ $\tilde{c}^3A_1$. The fluorescing transition of $\tilde{c}^3A_1\ (5a_1)^{-1} \rightarrow \tilde{a}^3B_2\ (4b_2)^{-1}$ is symmetry-allowed, while the $\tilde{c}^3A_1\ (5a_1)^{-1} \rightarrow \tilde{b}^3A_2\ (1a_2)^{-1}$ transition is symmetry-forbidden. From the Franck−Condon consideration,

$$NO_2^+\ \tilde{c}^3A_1\ (2,0,0) \rightarrow NO_2^+\ \tilde{a}^3B_2\ (n_1,2,0) + h\nu_f\ (\sim 300\ \text{nm}) \quad (12)$$

is expected to take place efficiently. The n_1 quantum numbers might spread over 1−3. Although we do not know the exact value of the transition moment for the radiative process (12), this radiative relaxation process seems to be responsible for the long lifetime of NO_2^+ measured with the photoionization of NO_2 at 71.5 nm. Another factor that we must consider as a source of this metastablity is that NO_2^+ $\tilde{c}^3A_1$ is free from any perturbation from repulsive potentials. Two repulsive triplet potentials, correlating with $O_2^+(X^2\Pi_g)$ + N(^4S), are expected to cross the $\tilde{c}^3A_1$ surface, but they do not belong to $^3A_1$.

The fifth and sixth excited triplet states, $\tilde{e}^3B_2$ and $\tilde{f}\ ^3A_1$, have fairly large amounts of electronic energies of 9.27 and 11.67 eV, respectively. Both processes of NO^+ + O and O^+ + NO take place. Specially, the $\tilde{e}^3B_2$ state is perturbed by a repulsive $^3B_2$ surface correlating with $O^+(^4S)$ + NO($X^2\Pi$). This must be the reason why 40% of NO_2^+ prepared in $\tilde{e}^3B_2$ dissociations into O^+ and NO.

Acknowledgment. We are grateful to Dr. Shinichi Nagaoka for his help in a part of this experiment. K. S. thanks the Institute for Molecular Science for providing an opportunity to work at the UVSOR facility and for financial support.

References and Notes

(1) Miyawaki, J.; Yamanouchi, K.; Tsuchiya, S. *Chem. Phys. Lett.* **1991**, *180*, 287.
(2) Buttnhoff, T. J.; Rohlfing, Eric A. *J. Chem. Phys.* **1993**, *98*, 5469.
(3) Ionov, S. I.; Brucker, G. A.; Jaques, C.; Chen, Y.; Wittig, C. *J. Chem. Phys.* **1993**, *99*, 3420.
(4) Georges, R.; Delon, A.; Jost, R. *J. Chem. Phys.* **1995**, *103*, 1732.
(5) Aoki, K.; Hoshina, K.; Shibuya, K. *J. Chem. Phys.* **1996**, *105*, 2228.
(6) Bryant, G. P.; Jiang, Y.; Martin, M.; Grant, E. R. *J. Chem. Phys.* **1994**, *101*, 7199.
(7) Koyano, I.; Tanaka, K. *J. Chem. Phys.* **1980**, *72*, 4858.
(8) Koyano, I.; Tanaka, K.; Kato, T.; Suzuki, S.; Ishiguro, E. Nuclear Instruments and Methods. *Phys. Res.* **1986**, *A246*, 507.
(9) Tanaka, K.; Kato, T.; Koyano, I. *J. Chem. Phys.* **1986**, *84*, 750.
(10) Brundle, C. R.; Neumann, D.; Price, W. C.; Evans, D.; Potts, A. W.; Streets, D. G. *J. Chem. Phys.* **1970**, *53*, 705.
(11) Price, W. C. In *Molecular Spectroscopy*; Hepple, P., Ed.; Elsevier: New York, 1968; Vol. 4, p 221.
(12) Handy, N. C.; Goddard, J. D.; Schaefer, H. F., III. *J. Chem. Phys.* **1979**, *71*, 426.
(13) Kimura, K.; Katsumata, S.; Achiba, Y.; Yamazaki, T.; Iwata, S. *Handbook of He I Photoelectron Spectra of Fundamental Organic Molecules*; Japan Scientific Society: Tokyo, 1980.
(14) Weissler, G. L.; Samson, J. A. R.; Ogawa, M.; Cook, G. R. *J. Opt. Soc. Am.* **1959**, *49*, 338.
(15) Dibeler, V. H.; Walker, J. A.; Liston, S. K. *J. Res. NBS−Phys. Chem.* **1967**, *71A*, 371.
(16) Mohammed, H. H.; Fournier, J.; Denson, J.; Vermeil, C. *Chem. Phys. Lett.* **1980**, *73*, 315.
(17) Chupka, W. A. Photoionization and fragmentation of polyatomic molecules. In *Chemical Spectroscopy and Photochemistry in the Vacuum-Ultraviolet*; Sandorfy, C., Ausloos, P. J., Robin, M. B., Eds.; D. Reidel: New York, 1973.
(18) Eland, J. H. D. Ion Fragmentation Mechanisms and Photoelectron Spectroscopy. *Electron Spectroscopy: Theory, Techniques and Applications*; Brundle, C. R., Baker, A. D., Eds.; Academic: New York, 1979; Vol. 3, Chapter 5.
(19) Slanger, T. G.; Black, G. *J. Chem. Phys.* **1978**, *68*, 1844.
(20) Zhu, Y. F.; Gordon, R. G. *J. Chem. Phys.* **1990**, *92*, 2897.
(21) Miller, R. L.; Kable, S. H. Houston, P. L.; Burak, I. *J. Chem. Phys.* **1992**, *96*, 332.